Fuel Processing Technology 217 (2021) 106818

Contents lists available at ScienceDirect

Fuel Processing Technology

journal homepage: www.elsevier.com/locate/fuproc

Research article

Efficient strategy of utilizing alkaline liquid waste boosting biomass chemical looping gasification to produce hydrogen

Wu Qin [a,1], Laixing Luo [a,1], Shubo Chen [a], Tahir Iqbal [b], Xianbin Xiao [a,*], Changqing Dong [a,*]

[a] National Engineering Laboratory for Biomass Power Generation Equipment & State Key Laboratory of Alternate Electrical Power System with Renewable Energy Sources, School of New Energy, North China Electric Power University, Beijing 102206, China
[b] Faculty of Agricultural Engineering & Technology, PMAS-Arid Agriculture University, Rawalpindi 46000, Pakistan

ARTICLE INFO

Keywords:
Hydrogen
Biomass
Chemical looping
Gasification
Liquid waste

ABSTRACT

The chemical looping gasification (CLG) between biomass and Fe_2O_3 be expressed as a potential hydrogen production technology as long as Fe_2O_3 could be effectively alkali-modified and enough steam could be supplied to the biomass gasification process. Therefore, a one-step strategy was developed herein by introduces KNO_3-containing acetic acid liquid waste to modify Fe_2O_3 and provide enough steam to improve the efficiency of hydrogen production from corn stalk. Experiments under different excess oxygen ratio (Ω), temperature (T) and potassium concentrations (m_{KNO3}) shows that these parameters have obvious effects on biomass CLG, and the highest hydrogen yield of 1.79 L is obtained at $\Omega = 0.2$, $T = 750$ °C and $m_{KNO3} = 8\%$. The kinetic and thermodynamic analysis further verifies that KNO_3-containing acetic acid liquid waste boosts biomass CLG for hydrogen generation. The proposed CLG strategy has dual advantages of waste treatment and energy conversion.

1. Introduction

Chemical looping gasification (CLG) between Fe_2O_3 and biomass to produce hydrogen has attracted the researcher's great attentions [1,2], since Fe_2O_3 is environmental friendliness, cheap, and heat-stable resource widely distributed on the earth with suitable redox thermodynamic properties for the CLG reaction to produce hydrogen [3,4]. The CLG schematic diagram is illustrated in Fig. 1. In the fuel reactor (FR), Fe_2O_3 partially oxidizes the pyrolysis/gasification products of biomass into CO, CO_2, and H_2, et al. During this process, Fe_2O_3 is reduced into FeO or Fe, which is oxidized at the same process by the steam to release H_2, high H_2/CO syngas can therefore be generated [3,5]. Then the solid mixture from FR is transferred to the air reactor (AR), where it is oxidized into Fe_2O_3 for the next CLG cycle.

In recent years, researches on CLG have mainly focused on reaction characteristics [6–9], multi-component carrier [10–12], reactor [13,14], system coupling [15–18] and process reinforcement [19,20]. Although it is found that alkali metal elements can significantly improve the activity of Fe_2O_3 for catalytic dissociation and gasification of biomass [21–24], as well as for coal chemical looping process [25,26], economical and feasible alkali modification of Fe_2O_3 still needs to be solved [27]. However, we tend to overlook the problem that a great amount of alkaline organic liquid waste is emitted from basic chemical raw material manufacturing, coal chemical, petrochemical, printing and dyeing, pesticide, and other industries. The alkaline organic liquid waste can be regarded as an important source of alkali (such as NaCl, Na_2SO_4, Na_2CO_3, K_2CO_3, and KNO_3) to modify Fe_2O_3, and the CLG of the liquid waste can not only recover the heat of organic components but also avoid the defects of secondary pollution (emission of NOx and CO_2) caused by traditional incineration methods [28–30]. Theoretically, the CLG of the mixture of alkaline organic liquid waste and biomass can perfectly solve the problems related to the activity of Fe_2O_3 and the insufficient gasification agent. However, there has not been an attempt at this strategy, and the reaction characteristics of this CLG reaction system is lack of research.

Therefore, experiments of corn stalk CLG using KNO_3-containing acetic acid aqueous solution as the simulated liquid waste under various conditions were performed to reveal the characteristics of the CLG reactions. Thermodynamics and reaction kinetics under the optimal operating conditions for high carbon conversion rate and H_2 yield are further discussed to prove the positive effect of introducing KNO_3-containing acetic acid solution for Fe_2O_3-based biomass CLG.

* Corresponding authors.
E-mail addresses: xiaoxianbin@ncepu.edu.cn (X. Xiao), dongcq@ncepu.edu.cn (C. Dong).
[1] Wu Qin and Laixing Luo contributes equally to this work.

https://doi.org/10.1016/j.fuproc.2021.106818
Received 2 November 2020; Received in revised form 12 January 2021; Accepted 10 March 2021
Available online 30 March 2021

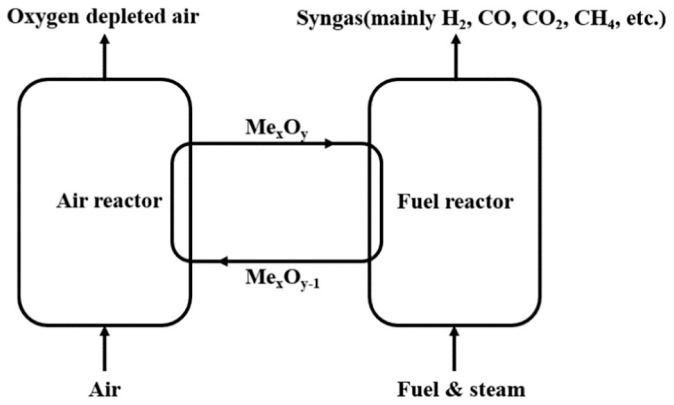

Fig. 1. Chemical looping gasification schematic diagram.

2. Methods

2.1. Materials

In the CLG system, feedstocks involved include the Fe_2O_3 supported on Al_2O_3 (Fe_2O_3/Al_2O_3) as the oxygen carrier (OC), corn stalks, and KNO_3-containing acetic acid aqueous solution. KNO_3-containing acetic acid aqueous solutions were prepared as the model liquid wastes. Fe_2O_3/Al_2O_3 with 60 wt% Fe_2O_3 and 40 wt% Al_2O_3 was prepared following the reported impregnation method [6], for which Al_2O_3 powder was mixed into saturated $Fe(NO_3)_3$ aqueous solution under continuous stirring. Then the mixture was dried for 8 h at 100 °C and the dried product was calcined at 900 °C for 1.5 h. The prepared Fe_2O_3/Al_2O_3 was ground into the powder with a diameter of 60–80 mesh for the CLG experiments. 6 wt% acetic acid solution prepared by dissolving acetic acid in deionized water was used to simulate the acetic acid liquid waste.

1 g corn stalk was dried at 110 °C under the flow of N_2 (62.5 mL/h) for 1.5 h. M_{ar} was calculated as follows:

$$M_{ar} = \frac{m - m_1}{m} \times 100 \quad (1)$$

where m and m_1 is the mass of corn stalk before and after drying, respectively.

1 g corn stalk was placed in a muffle furnace and calcined at 500 °C for 0.5 h and then calcined at 815 °C for 1 h. Finally, the corn stalk was dried at 500 °C for 1.5 h. A_{ar} was calculated as follows:

$$A_{ar} = \frac{m_2}{m} \times 100 \quad (2)$$

where m_2 is the mass of corn stalk after calcining and drying.

1 g corn stalk was calcined at 920 °C for 7 min. A_{ar} was calculated as follows:

$$V_{ar} = \frac{m - m_3}{m} \times 100 - M_{ar} \quad (3)$$

where m_3 is the mass of corn stalk after calcining.

F_{ar} was calculated as follows:

$$F_{ar} = 100 - V_{ar} - A_{ar} - M_{ar} \quad (4)$$

0.2 g corn stalk was put into a heating tube and calcined at 800 °C for 10 min under the flow of O_2 (120 mL/min). Then, an experiment under the same conditions without corn stalk was performed. C_{ar} was calculated as follows:

$$C_{ar} = \frac{12}{44} \times \frac{m_4}{m} \times 100 \quad (5)$$

H_{ar} was calculated as follows:

$$H_{ar} = \frac{2}{18} \times \frac{m_5 - m_6}{m} \times 100 - 0.1119 M_{ar} \quad (6)$$

Table 1
Proximate analysis of the corn stalk.

	V_{ar}	F_{ar}	A_{ar}	M_{ar}
Proportion of quality (%)	67.42	12.94	9.35	10.29

Note: *A*, *M*, *V*, and *F* are the ash, moisture, volatile and fixed carbon in corn stalk, respectively, and the meaning of subscript "ar" is "as received".

Table 2
Ultimate analysis of the corn stalk.

	C_{ar}	H_{ar}	O_{ar}	N_{ar}	S_{ar}	A_{ar}	M_{ar}
Proportion of quality (%)	41.14	5.94	32.54	0.58	0.17	9.35	10.29

Note: C_{ar}, H_{ar}, N_{ar}, O_{ar} and S_{ar} are the proportion of quality of carbon, hydrogen, nitrogen, and oxygen, and sulfur in the corn stalks, respectively.

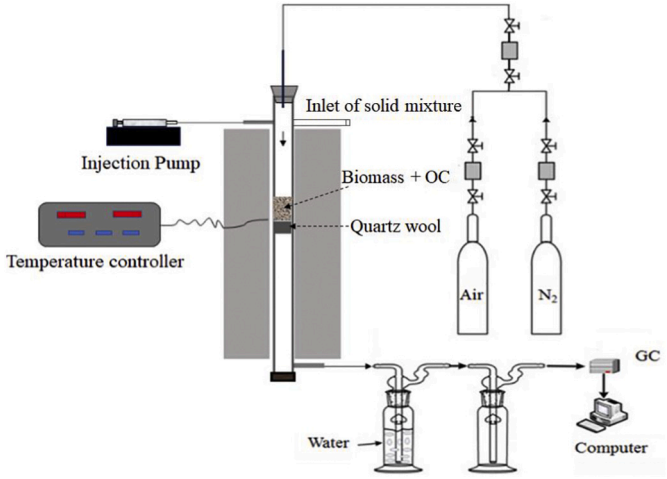

Fig. 2. Schematic arrangement of the CLG system.

where m_4 and m_5 is the increase in the weight of the U-shaped tube that absorbs CO_2 and H_2O, respectively. And m_6 is the increase in the weight of the U-shaped tube that absorbs H_2O in the experiment without corn stalk.

5 mL concentrated sulfuric acid with a specific gravity of 1.84 was added to 0.2 g corn stalk, the solution was diluted and then distilled. After the distillation was completed, the solution was titrated with 0.025 mol/L sulfuric acid standard solution. Then, an experiment under the same conditions with 0.2 g sucrose was performed.

N_{ar} was calculated as follows:

$$N_{ar} = \frac{0.05 \times (V_1 - V_2)}{m} \times \frac{14}{1000} \times 100 \quad (7)$$

where V_1 and V_2 is the volume of the standard sulfuric acid solution before and after the experiment with 0.2 g sucrose, respectively.

1 g corn stalk was mixed with 3 g Eschka reagent, where the mass ratio of MgO to $NaCO_3$ in Eschka reagent is 2:1. The mixture was calcined at 850 °C for 2 h. The mixture was diluted after cooling and excess $BaCl_2$ was added to the solution. Then, an experiment under the same conditions without corn stalk was performed.

S_{ar} was calculated as follows:

$$S_{ar} = \frac{m_7 - m_8}{m} \times \frac{32}{233} \times 100 \quad (8)$$

where m_7 and m_8 is the mass of $BaSO_4$ and the mass of $BaSO_4$ in the experiment without corn stalk, respectively.

The O_{ar} was calculated as follows:

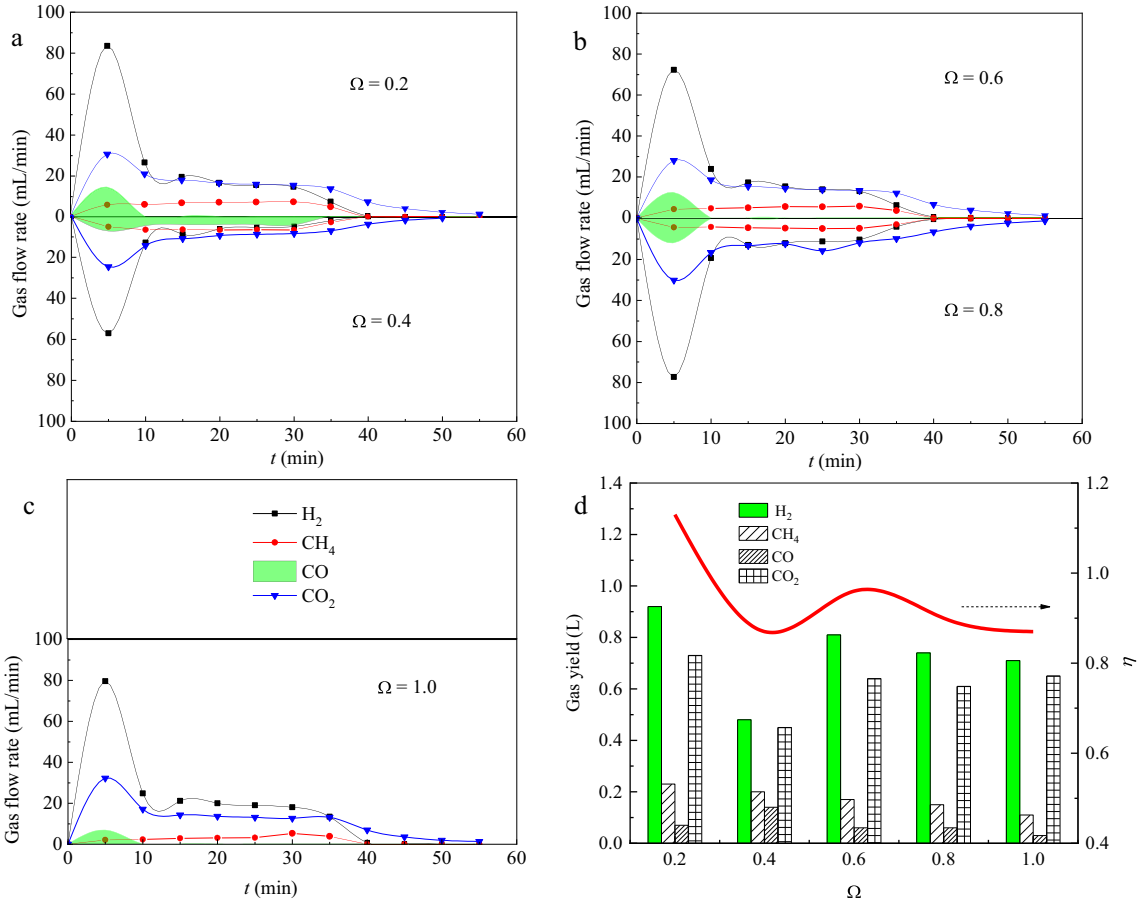

Fig. 3. Volume flow rate for the generated gases in the CLG process under $T = 800$ °C, $m_{KNO3} = 8\%$ and different Ω of a) 0.2 and 0.4, b) 0.6 and 0.8, c) 1.0. And d) Total gas yield and carbon conversion under $m_{KNO3} = 8\%$, $T = 800$ °C and different Ω.

$$O_{ar} = -100 - C_{ar} - H_{ar} - N_{ar} - S_{ar} - A_{ar} - M_{ar} \quad (9)$$

According to Table 1 and Table 2, the molecular formula of corn stalk can be approximated as $C_6H_{10}O_5$.

2.2. Performance and analysis

The CLG experimental system includes a syringe pump, a tube furnace, a gas inlet system, a quartz reaction tube, a dryer, a condenser, and a gas chromatograph (Agilent 490Micro GC). Fig. 2 illustrates the flow diagram of the CLG experiment. To perform the CLG experiments, N_2 with the flowing rate of 160 mL/min was continuously introduced into the quartz reaction tube of 18 mm inner diameter and 900 mm high, which was fixed in an electric stove. Once the predetermined reaction temperature had been reached, the mixture of Fe_2O_3/Al_2O_3 and corn stalk was immediately poured onto the quartz cotton set in the middle of the tube. Concurrently 10 mL of 6 wt% acetic acid solution containing different mass fractions of KNO_3 (6%, 8%, 10%) was injected through an injection pump into the quartz reaction tube at the rate of 0.333 mL/min. The feed rate of N_2 in the quartz reaction tube was 160 mL/min. The product gas was analyzed by an on-line gas chromatograph.

2.3. Data evaluation

Based on the nitrogen balance principle, the flow rate of outlet gas at the time (t), Q_t, was calculated as follows:

$$Q_t = \frac{Q_{N_2}}{1 - x_{H_2} - x_{CO} - x_{CH_4} - x_{CO_2}} \quad (10)$$

where Q_{N_2} is the inlet N_2 flow rate of 160 mL/min, x_{H_2}, x_{CO}, x_{CH_4} and x_{CO_2} is the volume fraction of the outlet gas H_2, CO, CH_4, and CO_2 at reaction time (t), respectively. The flow rate for each outlet gas at reaction time (t) was calculated as follows:

$$Q_{H_2}(t) = Q_t \times x_{H_2} \quad (11)$$

$$Q_{CO}(t) = Q_t \times x_{CO} \quad (12)$$

$$Q_{CH_4}(t) = Q_t \times x_{CH_4} \quad (13)$$

$$Q_{CO_2}(t) = Q_t \times x_{CO_2} \quad (14)$$

Then the total volume of the generated gas could be calculated as follows:

$$V_{H_2} = \int Q_{H_2}(t)dt \quad (15)$$

$$V_{CO} = \int Q_{CO}(t)dt \quad (16)$$

$$V_{CH_4} = \int Q_{CH_4}(t)dt \quad (17)$$

$$V_{CO_2} = \int Q_{CO_2}(t)dt \quad (18)$$

Carbon conversion rate, η_C, could be calculated as follows:

$$\eta_C = \frac{(V_{CO} + V_{CH_4} + V_{CO_2}) \times \frac{273}{273+60}}{22.4 \times (n_{fuel})} \quad (19)$$

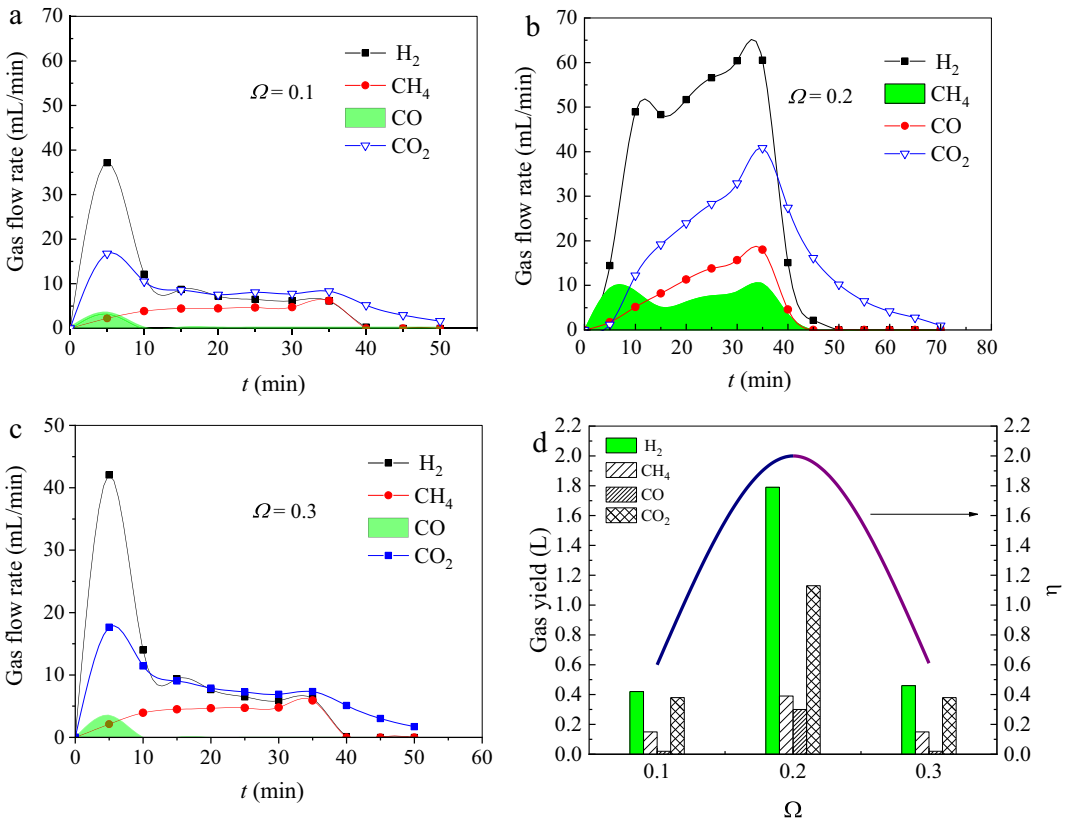

Fig. 4. Volume flow rate for the generated gases in the CLG process under $T = 750$ °C, $m_{KNO_3} = 8\%$ and different Ω of a) 0.1, b) 0.2 and c) 0.3.And d) total gas yield and carbon conversion under $m_{KNO_3} = 8\%$, $T = 750$ °C and different Ω.

Oxygen excess ratio (Ω) was calculated as follows:

$$n_{O_2} = 0.5 \times \left(\frac{C_{ar}}{12} + \frac{H_{ar}}{4} + \frac{S_{ar}}{32} - \frac{O_{ar}}{32}\right) \quad (20)$$

$$\Omega = \frac{0.4 \times m_{OC}}{160 \times n_{O_2}} \quad (21)$$

where C_{ar}, H_{ar}, S_{ar} and O_{ar} is the proportion of quality of carbon, hydrogen, sulfur, and oxygen in the corn stalks, respectively, and the meaning of subscript "ar" is "as received". m_{OC} is the mass of the OC.

3. Results and discussion

3.1. Gasification reaction characteristics under different Ω

Oxygen excess ratio (Ω) is defined as the ratio of the lattice oxygen in the OC to the oxygen consumed for complete oxidation of the fuel [31]. Ω acts as one of the most important factors affecting the CLG process. The effects of Ω (ranging from 0.2 to 1.0) on the biomass CLG driven by KNO_3-containing acetic acid were investigated under $T = 800$ °C and $m_{KNO_3} = 8\%$. The volume flow rate curves of the generated gas are shown in Fig. 3, More CH_4, CO_2, and CO are generated at $\Omega = 0.2$ than the other cases, since the increase of Ω favors the oxidation reactions (R6–R8) leading to the reduction of these gases [32]. The maximum H_2 flow rate reaches 83.47 mL/min at $\Omega = 0.2$, and the obvious H_2 flow rate at around 5 min could be attributed to the steam reforming reactions (R2–R5) [33,34]. During the first 10 min of the reaction, H_2 and CO_2 act as the main products, while CH_4 mainly derives from the pyrolysis of biomass and acetic acid (R1) keeping at a low proportion.

$$C_6H_{10}O_5 + CH_3COOH \rightarrow H_2 + CO + C_nH_m + CO_2 + C + char + H_2O \quad (R1)$$

$$H_2O + C/char \rightarrow H_2 + CO/CO_2 \quad (R2)$$

$$CH_3COOH + Fe_2O_3 + H_2O \rightarrow CO/CO_2 + H_2 + (CH_4) + Fe_2O_{3-x} \quad (R3)$$

$$C_6H_{10}O_5 + Fe_2O_3 + H_2O \rightarrow CO/CO_2 + H_2 + (CH_4) + Fe_2O_{3-x} \quad (R4)$$

$$Fe_2O_{3-x} + H_2O \rightarrow Fe_3O_4 + H_2 \quad (R5)$$

$$CH_4 + Fe_2O_3 \rightarrow CO_2 + H_2O + Fe_2O_{3-x} \quad (R6)$$

$$H_2 + Fe_2O_3 \rightarrow H_2O + Fe_2O_{3-x} \quad (R7)$$

$$CO + Fe_2O_3 \rightarrow CO_2 + Fe_2O_{3-x} \quad (R8)$$

$$CO + H_2O \rightarrow CO_2 + H_2 \quad (R9)$$

$$CH_4 + H_2O \rightarrow H_2 + CO \quad (R10)$$

$$CO_2 + C \rightarrow CO \quad (R11)$$

In Fig. 3d, $\Omega = 0.2$ contributes to the highest H_2 yield of 0.98 L. Under the case of $\Omega = 0.2$, Fe_2O_3 can be reduced into FeO and Fe [35]. With the participation of water vapor, the reaction R5 will be significantly improved to promote the generation of H_2 [34,35]. But with the increase of Ω, the proportion of the oxidation reaction R7 is higher than that of the H_2 generation reactions, resulting in a decrease of H_2 production [32,36]. When the Ω is 0.2, the content of CO is maintained at a relatively low level, and the maximum output is 71.7 mL since CO is easily oxidized by the OC following the R9 reaction [37] showing the highest output of CO_2 (0.73 L) and the highest η_C of 1.13. However, the fixed carbon in the biomass coke has not been further oxidized, which resulted in the drop of η_C greatly. As the Ω increases, more abundant lattice oxygen oxidizes the synthesis gas to water and inhibits the water

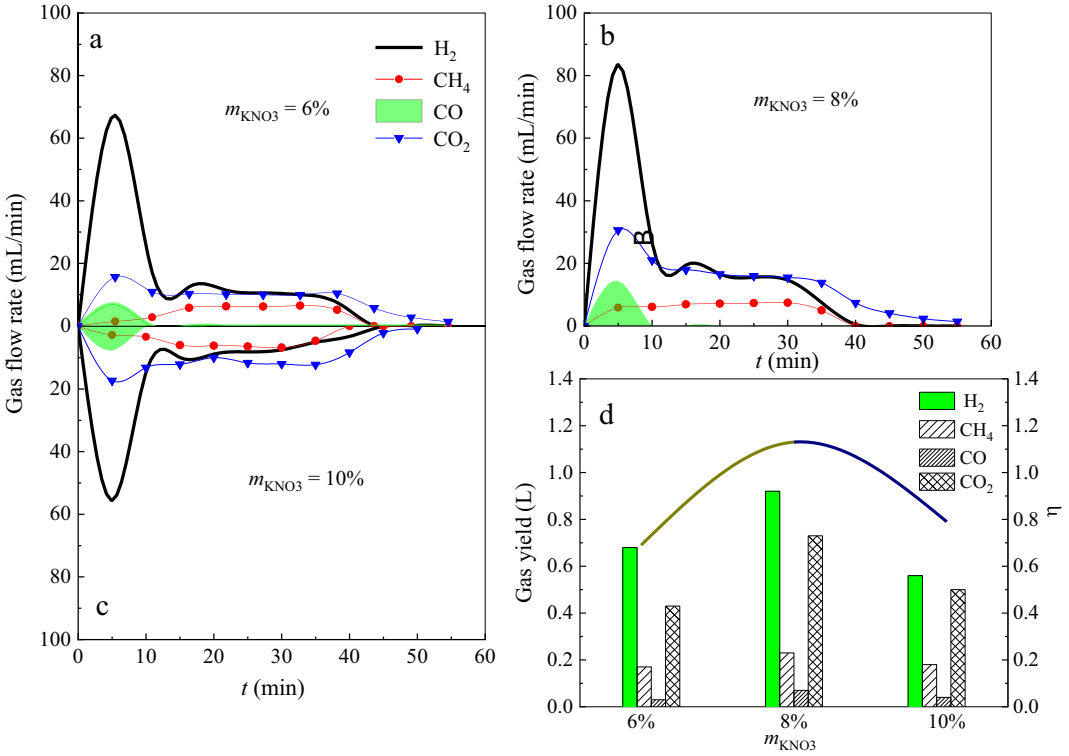

Fig. 5. Volume flow rate for the generated gases in the CLG process under $T = 800$ °C, $\Omega = 0.2$ and different m_{KNO3} of a) 6%, b) 8% and c) 10%.And d) total gas yield and carbon conversion under $\Omega = 0.2$, $T = 800$ °C and different m_{KNO3}.

vapor conversion reaction, which is not conducive to carbon conversion.

Fig. 4 shows the volume flow rate for the generated gases in the CLG process under $T = 750$ °C, $m_{KNO_3} = 8\%$ and different Ω. The H_2 volume flow rate under Ω of 0.2 can maintain an upward trend from 5 min and reach a maximum value at 35 min, 59.9 mL/min. Since the dripping of the liquid waste, the proportion of R2 [38], R5, and R9 is enhanced, resulting in high H_2 production. In Fig. 4d, at 750 °C and $\Omega = 0.2$, the H_2 yield is the highest, reaching 1.79 L, and the η_C is the highest, reaching 2.0. When the Ω increases to 0.3, the OC oxidizes the synthesis gas changing the conversion of fixed carbon and reducing the quality of syngas.

3.2. Gasification reaction characteristics under different potassium concentrations

The effect of m_{KNO_3} (6%, 8%, 10%) on CLG was studied at $\Omega = 0.2$ and $T = 800$ °C. As shown in Fig. 5, when $m_{KNO_3} = 8\%$, the output of H_2 and CO_2 is higher than in other cases, where the peak volume flow rate of H_2 and CO_2 is 85 mL/min and 31 mL/min, respectively. Appropriate m_{KNO_3} favors the carbon/steam reaction (R2), the Boundouard reaction (R11), and the steam reforming of methane (R10) [39,40], for which KNO_3 not only activates the OC by accelerating the lattice oxygen transfer [41] but also releases gas affecting the dispersibility and pore structure of OC and reacting with char accumulated on the surface of OC, hence improving the gasification process [42]. However, excess m_{KNO_3} will tend to form the molten salt and deposited on the surface of OC blocking the active sites and hindering the water vapor from entering the pores of OC [43] decreasing the lattice oxygen transfer efficiency and the reactivity [44]. In Fig. 5d, the highest output of each gas and the corresponding η_C under $m_{KNO_3} = 8\%$, indicating that KNO_3 of 8% shows a positive catalytic effect on the OC [45].

$$KNO_3 + C \rightarrow KNO_2 + K_2O + CO_2 + N_2 \quad \text{(R12)}$$

$$KNO_3 \rightarrow KNO_2 + K_2O + O_2 \quad \text{(R13)}$$

3.3. Gasification reaction characteristics at different temperatures

To study the effect of temperature on CLG, the experiment was carried out under the condition of $\Omega = 0.2$, $m_{KNO3} = 8\%$ and various temperatures. As shown in Fig. 6, the gas output at $T = 750$ °C is higher than that at 700 °C, 800 °C, and 850 °C. For the case of $T = 750$ °C, KNO_3 can also significantly activate the OC promoting the gasification reaction, while the reactions R2, R9, R10 [46,47] dominate the gasification conversion reaction [48] and the reduced OC show higher activity [49] to accelerate the reaction R5 [50] presenting higher H_2 generation rate than H_2 consumption rate. For the case of $T = 700$ °C, OC presents to be inactive enough for gasification. When the temperature increased to 800 °C, the oxidation effect of OC is stronger than the reduction effect, which causes the conversion of more H_2 into H_2O, while the oxidation of more CH_4 and CO occurs [48]. Further increase in temperature to 850 °C decreases the output of all gases. Accordingly, differing from that T = 750 °C contributes to the total H_2 yield of 3.61 L and the η_C of 2 at $\Omega = 0.2$ and $m_{KNO3} = 8\%$, lower and a higher temperature is not conducive to gasification and reforming reactions decreasing the gas yield and η_C. [51].

3.4. Characteristics of gasification reaction under different oxygen sources

To study the effect of different oxygen sources on CLG, experiments were carried out with the same quality of OC and Al_2O_3 at 750 °C, $\Omega = 0.2$ and $m_{KNO_3} = 8\%$. As shown in Fig. 7, the CLG reaction between Fe_2O_3/Al_2O_3 and biomass drove by acetic acid liquid waste generated more CO_2, CO H_2, and CH_4 than those from the CLG using Al_2O_3 as the OC [12,52]. Besides, the higher volume fraction of CO_2 indicates that the lattice oxygen of Fe_2O_3 can oxidize the combustible gas into CO_2. As a result, while Al_2O_3 contributes to the η_C of only 35%, Fe_2O_3/Al_2O_3 promotes the CLG process showing the η_C of about 100%.

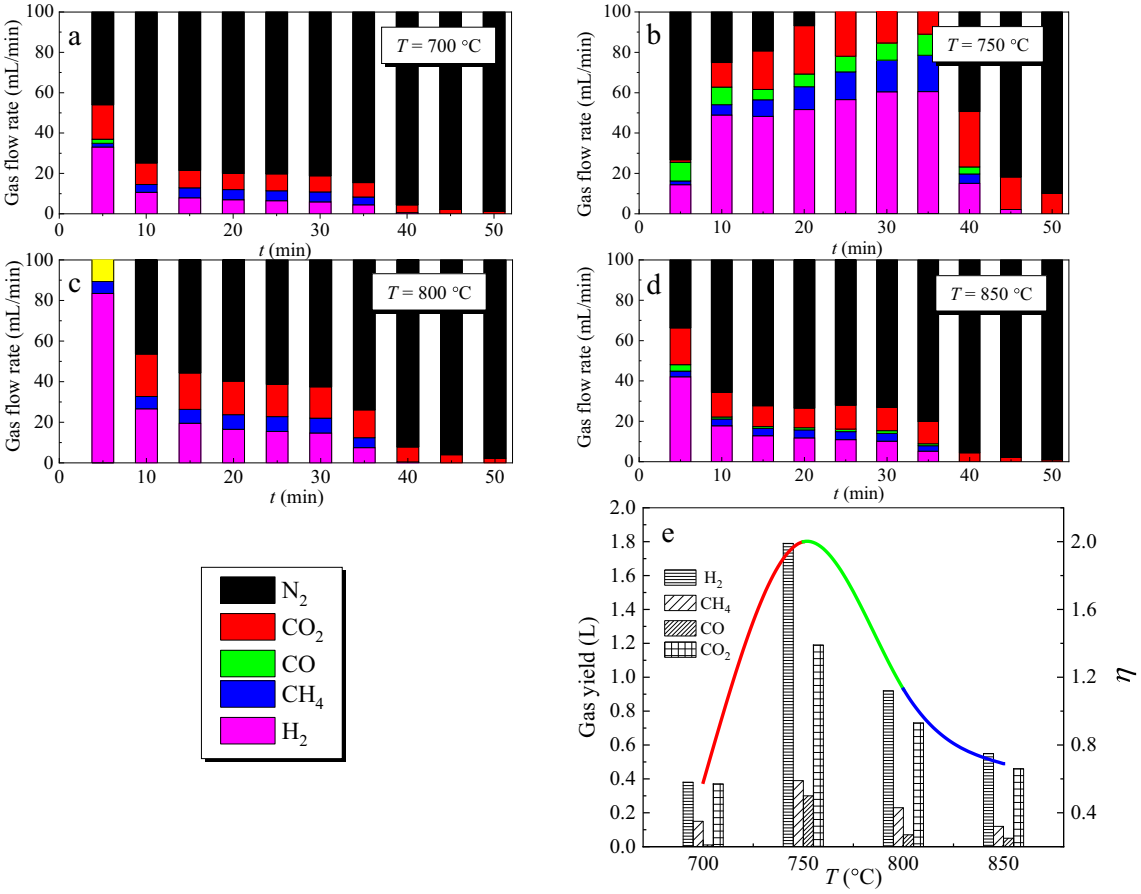

Fig. 6. Volume flow rate for the generated gases in the CLG process under $m_{KNO3} = 8\%$, $\Omega = 0.2$ and different temperature of a) 700 °C, b) 750 °C, c) 800 °C, d) 850 °C. And e) total gas yield and carbon conversion under $\Omega = 0.2$, $m_{KNO3} = 8\%$ and different temperatures.

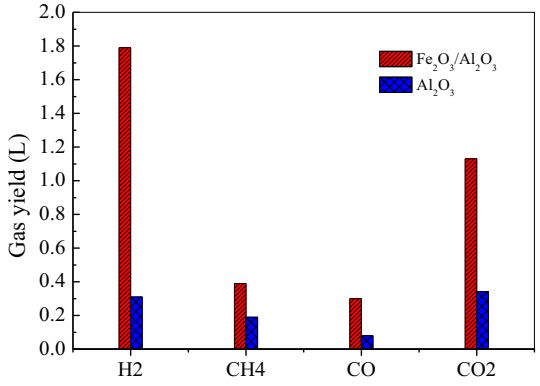

Fig. 7. Comparison of gas production volumes of various syngas under different oxygen sources.

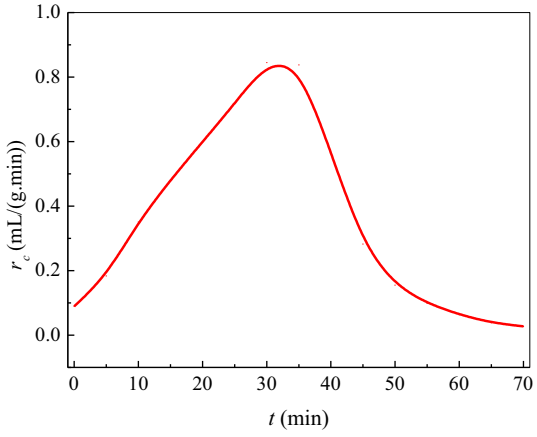

Fig. 8. The calculated r_c for CLG under $T = 750$ °C, $\Omega = 0.2$ and $m_{KNO_3} = 8\%$.

3.5. Kinetics analysis

Kinetics analysis was performed for CLG under the optimized case, where $T = 750$ °C, $m_{KNO_3} = 8\%$ and $\Omega = 0.2$. In reference to the previous report [3], the volume of the carbon-containing flue gas, V_C, could be calculated as follows:

$$V_C = V_{CH_4} + V_{CO} + V_{CO_2} \quad (22)$$

The molar amount of carbon converted during the reaction was calculated as follows:

$$n_C = \frac{V_C}{24.45} \quad (23)$$

Carbon conversion reaction rate, r_c, was calculated as follows:

$$r_c = \frac{dn_c}{m_{oc}dt} \quad (24)$$

where m_{oc} is the mass of the used Fe_2O_3/Al_2O_3. The calculated r_c for CLG under $\Omega = 0.2$, $T = 750$ °C and $m_{KNO_3} = 8\%$, is depicted in Fig. 8. r_c increases first and reaches the maximum value of 0.845 mL/(g•min).

Table 3
Related thermodynamic parameters, including standard molar reaction enthalpy ($\Delta_r H_m^\theta$) and molar isobaric hot melt ($C_{m,\ p}$), for various components.

Physical parameters	Unit	Value
$\Delta_r H_m^\theta(Fe, 298.15\ K)$	kJ/mol	0
$\Delta_r H_m^\theta(Fe3O4, 298.15\ K)$	kJ/mol	−1118.38
$\Delta_r H_m^\theta(FeO2, 98.15\ K)$	kJ/mol	−271.96
$\Delta_r H_m^\theta(Fe2O3, 298.15\ K)$	kJ/mol	−824.25
$\Delta_r H_m^\theta(C2H6O(l), 298.15\ K)$	kJ/mol	−236.92
$\Delta_r H_m^\theta(CO2, 298.15\ K)$	kJ/mol	−393.51
$\Delta_r H_m^\theta(CO, 298.15\ K)$	kJ/mol	−110.525
$\Delta_r H_m^\theta(CH4, 298.15\ K)$	kJ/mol	−74.81
$\Delta_r H_m^\theta(H2O(l), 298.15\ K)$	kJ/mol	−241.82
$C_{m,\ p}(Fe3O4, 298.15\ K)$	J/(mol·K)	143.43
$C_{m,\ p}(Fe2O3, 298.15\ K)$	J/(mol·K)	C_p = 4E -07 T^3–0.0007T^2 + 0.5649 T - 9.9088
$C_{m,\ p}(C2H6O, 298.15\ K)$	J/(mol·K)	Cp = 0.145 T + 104.12
$C_{m,\ p}(CO2, 298.15\ K)$	J/(mol·K)	$C_p = 26.75 + 42.258 \times 10^{-3} \times T$-14.25 × $10^{-6} \times T^2$
$C_{m,\ p}(CO, 298.15\ K)$	J/(mol·K)	$C_p = 26.537 + 7.6831 \times 10^{-3} \times T$-1.172 × $10^{-6} \times T^2$
$C_{m,\ p}(CH4, 298.15\ K)$	J/(mol·K)	$C_p = 14.15 + 75.496 \times 10^{-3} \times T$-17.99 × $10^{-6} \times T^2$
$C_{m,\ p}(H2O, 298.15\ K)$	J/(mol·K)	$C_p = 30 + 10.7 \times 10^{-3} \times T$-2.022 × $10^{-6} \times T^2$
$C_{m,\ p}(corn\ stalk, 298.15\ K)$	J/(mol·K)	63.43

Then r_c decreases continuously due to the difficulty oxidating the fixed carbon remaining in the biomass.

3.6. Thermal dynamics analysis

The balance of C and H was calculated according to Eqs. (25) and (26), respectively. During the CLG, the fuel and steam are introduced into the FR, then these components flow out of the reactor as product gas ($N_{i,\ CH4,\ out}$, $N_{i,\ CO2,\ out}$, $N_{i,\ CO,\ out}$, $N_{H,\ H2,\ out}$), steam ($N_{i,\ H2O,\ out}$) and remain as solid residuals ($N_{C,\ solid\ residuals,\ out}$) after reaction [53].

$$N_{H,CH3COOH,in} + N_{H,biomass,in} + N_{H,H2O,in} = N_{H,H2O,out} + N_{H,H2,out} + N_{H,CH4,out} \quad (25)$$

$$N_{C,biomass,in} + N_{C,CH3COOH,in} = N_{C,CH4,out} + N_{C,CO2,out} + N_{C,CO,out} + N_{C,solid\ residuals,out} \quad (26)$$

where $N_{i,\ j,\ in/out}$ is the total molar of component "i" (C, H) in "j" (H_2O, biomass, etc.) as "in" (input) or "out" (output) of the fuel reactor. (mol).

The heat balance of the system was further analyzed, which would determine the stable operation of the CLG system. Thermal dynamics analysis was performed according to the electron balance between biomass and the product syngas [19,20]. Thermodynamic parameters [54] are listed in Table 3. The chemical looping reaction process of acetic acid can be written as the following formula:

$$C_2H_4O_2 + 1.2Fe_2O_3 \rightarrow 0.77CH_4 + 1.23CO_2 + 0.46H_2O + 0.42Fe_3O_4 + 0.73FeO\ (\Delta H_{mol} = 57.88\ kJ/mol)$$

This step is endothermic, for which 0.013 mol Fe_2O_3 was reduced and the total reaction enthalpy is 0.627 kJ. Then, corn stalk CLG reaction can be concluded as:

$$C_{1.7}H_3O + 0.15Fe_2O_3 + 1.05H_2O \rightarrow 2.43H_2 + 0.24CH_4 + 0.42CO + 1.04CO_2 + 0.28FeO + 0.02Fe\ (\Delta H = -119.08\ kJ/mol)$$

This step is an exothermic reaction, where 0.0043 mol Fe_2O_3 was reduced and the calculated reaction enthalpy is −0.512 kJ. Therefore, the total reaction enthalpy for reforming the biomass is 0.115 kJ. However, the complete CLG system includes the fuel gasification process and the reduced OC oxidation process. Oxidation of 0.0046 mol Fe_3O_4, 0.0159 mol FeO, and 0.0006 mol Fe can release the heat of −3.02 kJ, which can balance the heat required for the gasification of acetic acid and biomass.

3.7. Structural characterizations

Fig. 9 depicts the X-ray diffraction (XRD) patterns and the scanning electron microscopy (SEM) imagines for the pure Fe_2O_3/Al_2O_3 and the K-modified Fe_2O_3/Al_2O_3. According to the XRD, the diffraction peaks correspond to a different facet of Fe_2O_3, which indicates that the pure Fe_2O_3/Al_2O_3 has a high degree of crystallinity. The absence of Al_2O_3 diffraction peak indicates that Al_2O_3 is covered by Fe_2O_3. The XRD pattern of Fe_2O_3/Al_2O_3 modified with 8% KNO_3 solution appears crystal planes of KNO_2 [200] and Al_2O_3. This may be due to the thermal decomposition of KNO_3 into KNO_2, which changes the distribution of Fe_2O_3 on the Al_2O_3 crystal plane. The SEM results show that, in comparison with the surface of Fe_2O_3/Al_2O_3, the K-modified Fe_2O_3/Al_2O_3 shows particles of different sizes on its rough surface. The rough surface can be attributed to the nitrogen-containing gas released from the thermal decomposition of KNO_3, which changes the pore structure and the distribution of Fe_2O_3. Besides, the regeneration and reaction stability of Fe_2O_3-based OC has been verified [55].

Fig. 10 further shows the SEM image, energy dispersive spectrometer (EDS) analysis, and XRD pattern for the K-modified Fe_2O_3/Al_2O_3 after the reaction. It can be observed that the rough surface and holes of the K-modified Fe_2O_3/Al_2O_3 sample were destroyed after the reaction, showing the traces of sintering among particles, which causes

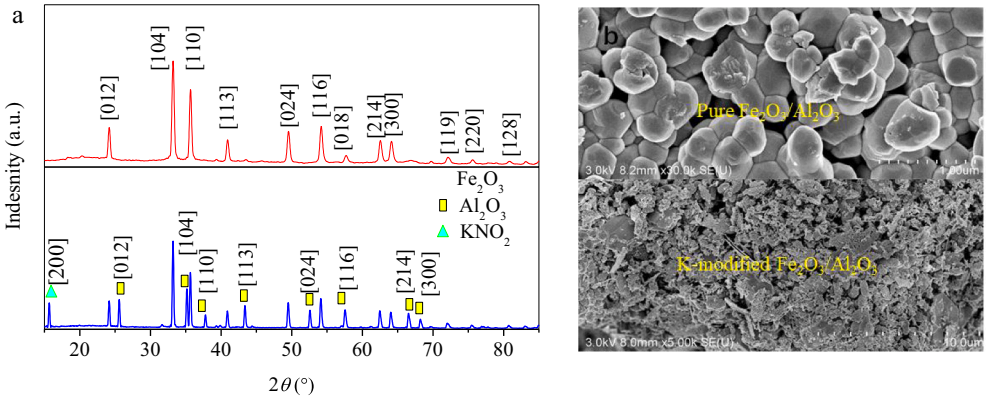

Fig. 9. XRD patterns a) and scanning electron microscopy (SEM) imagine b) for the pure Fe_2O_3/Al_2O_3 and the K-modified Fe_2O_3/Al_2O_3.

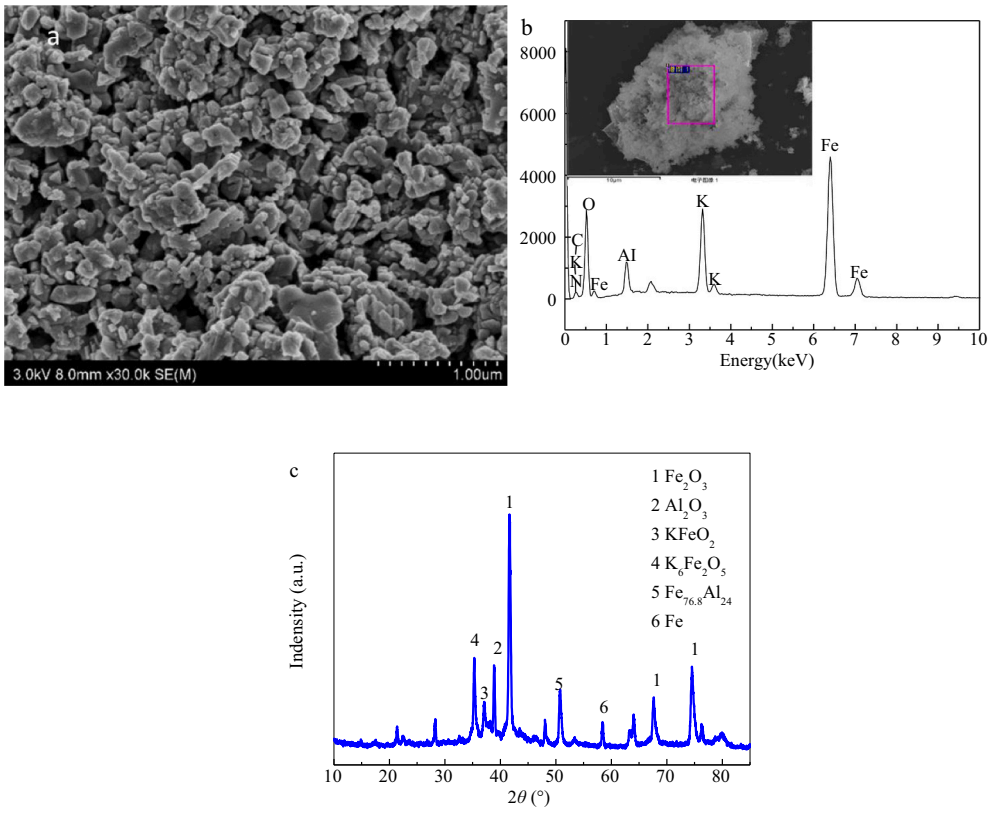

Fig. 10. The SEM image a), EDS analysis b), and XRD pattern c) for the K-modified Fe_2O_3/Al_2O_3 after the reaction.

Table 4
The ICP-MS analysis of for the K-modified Fe_2O_3/Al_2O_3 after the reaction.

	Al	Fe	K
Proportion of quality (%)	13.01	42.58	7.15

agglomeration and porosity reduction of the overall structure. The EDS results show that the sample contains Fe, K, Al, O, N, and C, where N would mainly correspond to KNO_2 as verified in Fig. 9a, and the small amount of C would derive from carbon deposition during the CLG process [56]. The calculated 7.15% K based on the inductively coupled plasma mass spectrometer (ICP-MS) analysis in Table 4 and the diffraction peak of K-Fe-O in Fig. 10c indicates that Fe_2O_3/Al_2O_3 can react with KNO_3, generating K-Fe-O compounds ($KFeO_2$ and $K_6Fe_2O_5$). K-Fe-O compounds have a spinel structure that is similar to the structure of β-Al_2O_3, which can improve the reactivity of OC [57].

4. Conclusions

This work revealed the effect of KNO_3-containing acetic acid solution on biomass CLG. The optimal parameters of $T = 750$ °C, $\Omega = 0.2$, and $m_{KNO3} = 8\%$ contribute to the highest H_2 yield of 3.58 L per gram of corn stalk and almost complete carbon conversion (with a small amount of C according to ICP-MS analysis). Thermodynamic and Reaction kinetics analysis further verified the possibility of introducing KNO_3-containing acetic acid solution to boost corn stalk CLG. The novel strategy of improving biomass CLG by using KNO_3-containing acetic acid liquid waste not only favors energy conversion but also treats organic liquid waste, achieving both energy effect and good environmental effect.

Declaration of Competing Interest

The authors declare that they have no known competing financial interests or personal relationships that could have appeared to influence the work reported in this paper.

Acknowledgments

The authors wish to thank the National Natural Science Foundation of China (51776071, 51776070), the Fundamental Research Funds for the Central Universities (2018ZD08, 2018MS034, 2016YQ07), and the National Key R & D Program of China (2016YFB0600205-04).

References

[1] S. Zhao, Y.C. Shi, K.R. Christopher, H. Jun, H.R. Asif, T. Gang, et al., Improvement of H_2-rich gas production with tar abatement from pine wood conversion over bi-functional $Ca_2Fe_2O_5$ catalyst: investigation of inner-looping redox reaction and promoting mechanisms, Appl. Energy 212 (2018) 931–943.
[2] Z. Liang, C. Zhuo, A.F. Jonathan, F. Liang-Shih, L.G. Jin, Metal oxide redox chemistry for chemical looping processes, Nat. Rev. Chem. 2 (2018) 349–364.
[3] Z. Huang, F. He, H. Zhu, D. Chen, K. Zhao, G. Wei, Thermodynamic analysis and thermogravimetric investigation on chemical looping gasification of biomass char under different atmospheres with Fe_2O_3 oxygen carrier, Appl. Energy 157 (2015) 546–553.
[4] I. Wang, G. Ji, Y. Turap, H. Nie, Z. Li, M. Zhao, W. Wang, A short-cut chemical looping hydrogen generation system by using iron-based material from steel industry, Chem. Eng. J. 394 (2020) 124882.
[5] K. Srirangan, M. Pyne, C. Perry, Biochemical and genetic engineering strategies to enhance hydrogen production in photosynthetic algae and cyanobacteria, Bioresour. Technol. 102 (2011) 85–89.
[6] M.A. Soria, B. Diogo, L.M. Madeira, Hydrogen production through steam reforming of bio-oils derived from biomass pyrolysis: thermodynamic analysis including in situ CO_2 and/or H_2 separation, Fuel 244 (2019) 184–195.
[7] Y. Wu, Y. Liao, G. Liu, X. Ma, Syngas production by chemical looping gasification of biomass with steam and CaO additive, Int. J. Hydrog. Energy 43 (2018) 19375–19383.
[8] G. Liu, Y. Liao, Y. Wu, X. Ma, Synthesis gas production from microalgae gasification in the presence of Fe_2O_3 oxygen carrier and CaO additive, Appl. Energy 212 (2018) 955–965.
[9] B. Dou, H. Zhang, Y. Song, L. Zhao, B. Jiang, M. He, et al., Hydrogen production from the thermochemical conversion of biomass: issues and challenges, Sustain. Energy Fuels 3 (2019) 314–342.

[10] D. Zeng, D. Cui, Y. Qiu, M. Li, L. Ma, S. Zhang, R. Xiao, Mn-Fe-Al-O mixed spinel oxides as oxygen carrier for chemical looping hydrogen production with CO_2 capture, Fuel 274 (2020) 117854.
[11] D. Zeng, F. Kang, Y. Qiu, D. Cui, M. Li, L. Ma, S. Zhang, R. Xiao, Iron oxides with gadolinium-doped cerium oxides as active supports for chemical looping hydrogen production, Chem. Eng. J. 396 (2020) 125153.
[12] A. Zheng, Y. Fan, G. Wei, K. Zhao, Z. Huang, Z. Zhao, H. Li, Chemical looping gasification of torrefied biomass using $NiFe_2O_4$ as an oxygen carrier for syngas production and tar removal, Energy Fuel 34 (2020) 6008–6019.
[13] N. Armbrust, G. Duelli-Varela, H. Dieter, G. Schenecht, Calcium looping cycle for hydrogen production from biomass gasification syngas: Experimental investigation at a 20 kWth dual fluidized bed facility, J. Ind. Eng. Chem. 54 (2015) 5624–5634.
[14] L. Yan, Y. Cao, X. Li, B. He, Characterization of a dual fluidized bed gasifier with blended biomass/coal as feedstock, Bioresour. Technol. 254 (2018) 97–106.
[15] Y. Yi, J. Ying, J. Zhao, Development on thermochemical energy storage based on CaO-based materials: a review, Sustainability 10 (2018) 2660.
[16] X. Zhao, D. Xing, N. Fu, B. Liu, N. Ren, Hydrogen production by the newly isolated Clostridium beijerinckii RZF-1108, Bioresour. Technol. 102 (2011) 8432–8436.
[17] M. Schmidt, M. Linder, Power generation based on the $Ca(OH)_2$/CaO thermochemical storage system-experimental investigation of discharge operation modes in lab scale and corresponding conceptual process design, Appl. Energy 203 (2017) 594–607.
[18] S. Chen, Z. Xue, D. Wang, W. Xiang, An integrated system combining chemical looping hydrogen generation process and solid oxide fuel cell/gas turbine cycle for power production with CO_2 capture, J. Power Sources 215 (2012) 89–98.
[19] W. Qin, S. Chen, B. Ma, J. Wang, J. Li, R. Liang, et al., Ethanol solution promoting cotton fiber chemical looping gasification for high H_2/CO ratio syngas, Int. J. Hydrog. Energy 44 (2019) 7149–7157.
[20] W. Qin, J. Wang, Q. Gao, G. Li, X. Chen, S. Chen, et al., Corn-stalk chemical looping combustion using tert-butanol waste solution, Energy Fuel 33 (2019) 1622–1630.
[21] S. Hosseinpour, M. Aghbashlo, M. Tabatabaei, H. Younesi, M. Mehrpooya, S. Ramakrishna, Multi-objective exergy-based optimization of a continuous photobioreactor applied to produce hydrogen using a novel combination of soft computing techniques, Int. J. Hydrog. Energy 42 (2016) 8518–8529.
[22] P. Searmsirimongkol, P. Rangsunvigit, M. Leethochawalit, S. Chavadej, Hydrogen production from alcohol distillery wastewater containing high potassium and sulfate using an anaerobic sequencing batch reactor, Int. J. Hydrog. Energy 36 (2011) 12810–12821.
[23] S. Zhang, L. Shen, J. Xiao, Catalytic combustion of coal using alkali and transition metals loaded on iron ore oxygen carrier, J. Fuel Chem. Technol. 40 (2012) 1179–1187.
[24] Y. Wang, X. Tian, H. Zhao, K. Liu, The use of a low-cost oxygen carrier prepared from red mud and copper ore for in situ gasification chemical looping combustion of coal, Fuel Process. Technol. 205 (2020) 106460.
[25] Z. Yu, T. Liu, C. Li, S. Guo, X. Zhou, Y. Chen, et al., Coal direct chemical looping hydrogen production with K-Fe-Al composite oxygen carrier, Int. J. Greenh. Gas Con. 75 (2018) 24–31.
[26] H. Ge, L. Shen, H. Gu, S. Jiang, Effect of co-precipitation and impregnation on K-decorated Fe_2O_3/Al_2O_3 oxygen carrier in chemical looping combustion of bituminous coal, Chem. Eng. J. 262 (2015) 1065–1076.
[27] M.A. Naeem, Optimization of the structural characteristics of CaO and its effective stabilization yield high-capacity CO_2 sorbents, Nat. Commerce 9 (2018) 2408.
[28] J. Chen, X. Jin, X. Hu, Present research and development trends of organic liquid waste incineration technology, Anhui Chem. Ind. 37 (2011) 9–11.
[29] J. Zhao, Z. Ma, Y. Chen, Migration of alkali metal salts of high salinity organic liquid waste in fluidized bed combustion, Energy Eng. 4 (2016) 51–55.
[30] N. Berguerand, A. Lyngfelt, Design and operation of a 10 kWth chemical-looping combustor for solid fuels e testing with south African coal, Fuel 87 (2008) 13–26.
[31] Z. Huang, Y. Zhang, J. Fu, L. Yu, M. Chen, S. Liu, et al., Chemical looping gasification of biomass char using iron ore as an oxygen carrier, Int. J. Hydrog. Energy 41 (2016) 17871–17883.
[32] J. Chen, K. Zhao, L. Zhao, F. He, Z. Huang, G. Wei, et al., Reaction schemes of barium ferrite in biomass chemical looping gasification for hydrogen-enriched syngas generation via an outer-inner looping redox reaction mechanism, Energy Convers. Manag. 189 (2019) 81–90.
[33] Y. Vos, M. Jacobs, P. Voort, I. Driessche, F. Snijkers, A. Verberckmoes, Sustainable iron-based oxygen carriers for chemical looping for hydrogen generation, Int. J. Hydrog. Energy 44 (2019) 1374–1391.
[34] G.R. Kale, B.D. Kulkarni, K.V. Bharadwaj, Chemical looping reforming of ethanol for syngas generation: a theoretical investigation, Int. J. Energy Res. 37 (2013) 645–656.
[35] L.-S. Fan, Chemical Looping Systems for Fossil Energy Conversions, Hoboken NJ USA, John Wiley & Sons Inc, 2010.
[36] Q. Liu, C. Hu, B. Peng, C. Liu, Z. Li, K. Wu, et al., High H_2/CO ratio syngas production from chemical looping co-gasification of biomass and polyethylene with CaO/Fe_2O_3 oxygen carrier, Energy Convers. Manag. 199 (2019) 111951.
[37] B.V.R.K. Prasad, J.L. Kuester, Process analysis of a dual fluidized bed biomass gasification system, Ind. Eng. Chem. Res. 27 (1988) 304–310.
[38] J. Alvarez, G. Lopez, M. Amutio, J. Bilbao, M. Olazar, Evolution of biomass char features and their role in the reactivity during steam gasification in a conical spouted bed reactor, Energy Convers. Manag. 181 (2019) 214–222.
[39] N. Xiao, H. Luo, W. Wei, Z. Tang, B. Hu, L. Kong, et al., Microwave-assisted gasification of rice straw pyrolytic biochar promoted by alkali and alkaline earth metals, J. Anal. Appl. Pyrolysis 112 (2015) 173–179.
[40] Z. Wang, P. Ouyang, L. Cui, B. Zong, G. Wu, Y. Zhang, Valorizing petroleum coke into hydrogen-rich syngas through K-promoted catalytic steam gasification, J. Energy Inst. 93 (2020) 2544–2549.
[41] T. Mattison, F. Hildor, Y. Li, C. Linderholm, Negative emissions of carbon dioxide through chemical-looping combustion (CLC) and gasification (CLG) using oxygen carriers based on manganese and iron, Mitig. Adapt. Strat. Gl. 25 (2020) 497–517.
[42] H. Wang, R. Shen, Y. Ye, L. Wu, Thermal behaviour and decomposition reaction kinetics of graphite/potassium nitrate, Chin. J. Energetic Mater. 20 (2012) 731–734.
[43] Y. Zhang, X. Gong, B. Zhang, W. Liu, M. Xu, Potassium catalytic hydrogen production in sorption enhanced gasification of biomass with steam, Int. J. Hydrog. Energy 39 (2014) 4234–4243.
[44] Z. Zhang, Y. Wang, L. Zhu, J. Li, F. Wang, G. Yu, Effects of Na_2CO_3/K_2CO_3 on chemical looping combustion using Fe_2O_3/Al_2O_3 as oxygen carrier, Chem. Eng. Technol. 43 (2020) 412–421.
[45] S. Xiao, J. Ma, X. Li, X. Chen, Review of the incineration process for the treatment of industrial liquid waste, Ind. Water Treat. 32 (2012) 16–19.
[46] L. Shen, Y. Gao, J. Xiao, Simulation of hydrogen production from biomass gasification in interconnected fluidized beds, Biomass Bioenergy 32 (2008) 120–127.
[47] M. Al-Zareer, I. Dincer, M.A. Rosen, Analysis and assessment of a hydrogen production plant consisting of coal gasification, thermochemical water decomposition and hydrogen compression systems, Energy Convers. Manag. 157 (2018) 600–618.
[48] C. Franco, F. Pinto, I. Gulyurtlu, I. Cabrita, The study of reactions influencing the biomass steam gasification process, Fuel 82 (2003) 835–842.
[49] A. Inayat, M.M. Ahmad, S. Yusup, M.I.A. Mutalib, Biomass steam gasification with in-situ CO_2 capture for enriched hydrogen gas production: a reaction kinetics modelling approach, Energies 3 (2010) 1472–1484.
[50] Z. Huang, G. Xu, Z. Deng, K. Zhao, F. He, D. Chen, et al., Investigation on gasification performance of sewage sludge using chemical looping gasification with iron ore oxygen carrier, Int. J. Hydrog. Energy 42 (2017) 25474–25491.
[51] M.R. Mahishi, D.Y. Goswami, Thermodynamic optimization of biomass gasifier for hydrogen production, Int. J. Hydrog. Energy 32 (2007) 3831–3840.
[52] M. Ortiz, P. Gayan, L. de Diego, F. Garcia-Labiano, A. Abad, M. Pans, Hydrogen production with CO_2 capture by coupling steam reforming of methane and chemical-looping combustion: use of an iron-based waste product as oxygen carrier burning a PSA tail gas, J. Power Sources 196 (2011) 4370–4381.
[53] J. Fuchs, J.C. Schmid, S. Müller, A.M. Mauerhofer, F. Benedikt, H. Hofbauer, The impact of gasification temperature on the process characteristics of sorption enhanced reforming of biomass, Biomass Convers. Bior. 10 (2020) 925–936.
[54] X.C. Fu, W.X. Shen, Physical Chemistry, Higher Education Press, Beijing, China, 2005, pp. 481–492.
[55] W. Qin, Y. Wang, C. Lin, X. Hu, C. Dong, Possibility of morphological control to improve the activity of oxygen carriers for chemical looping combustion, Energy Fuel 29 (2015) 1210–1218.
[56] Y. Wu, Y. Liao, G. Liu, X. Ma, H. Zhang, Reactivity investigation on biomass chemical looping conversion for syngas production, J. Energy Inst. 92 (2019) 1137–1148.
[57] Y. Liu, X. Zhang, M. Gao, X. Hu, Q. Guo, Effect of coal ash on Fe-based oxygen carrier in coal char chemical looping gasification, Int. J. Chem. React. Eng. 17 (2019), https://doi.org/10.1515/ijcre-2018-0270.